



Studying the Relation of the Residual Stresses in the Ballast Layer to the Elastic Wave Propagation

Mykola Sysyn¹ · Ulf Gerber¹ · Jianxing Liu² · Szabolcs Fischer³ 

Accepted: 3 July 2022
© The Author(s) 2022

Abstract

During track construction or ballast bed maintenance, ballast layer compaction quality plays an essential role in the following track irregularity accumulation, its lifecycle, and maintenance costs. The ballast compaction process is characterized by its compaction and the accumulation of the stressed state. The elastic wave propagation methods are an effective way for the identification of the ballast bed compaction properties. The paper presents the theoretical and experimental studies of the ballast consolidation under the vibration loading of the sleeper. The practical laboratory study is given by the 1:2.5 scaled physical model of one sleeper and the corresponding ballast layer box. The measurements of ballast pressure and deformations under the vibration loading in the ballast layer and the photogrammetric recording of the ballast flow are carried out. The measurements demonstrate the accumulation of the residual stresses under the ballast layer. Furthermore, the measurements of elastic wave time of flight (ToF) using the shakers under the sleeper and acceleration sensors under the ballast show the substantial increase of the ToF velocities after the tamping process. Moreover, the distribution of the velocities along the sleeper is spatially inhomogeneous. The numeric simulation using the discrete element method (DEM) of the tamping and the testing processes proves the inhomogeneous wave propagation effect. The modeling shows that the main reason for the wave propagation inhomogeneity is the accumulated residual stress distribution and the minor one – the compaction density. Additionally, a method for identifying wave velocity spatial distribution is developed by wave tracing the inhomogeneous medium. The procedures allow ballast identification in the zones outside the shakers.

Keywords Railway ballast · Compaction · Residual stress · DEM modeling · Elastic wave propagation

✉ Szabolcs Fischer
fischersz@sze.hu

Extended author information available on the last page of the article

1 Introduction

The ballast layer is a track superstructure part with a quick accumulation of residual deformations that influences the geometrical quality of railway tracks during their lifecycle. The 40–70 million ton standard ballast tamping cycles are the shortest maintenance cycles for other track elements (Lichtberger 2005). Therefore, the lifecycle cost distribution for European conditions is 20% maintenance costs, 33% operational hindrance costs, and 47% depreciation costs (Lichtberger 2005; Fendrich and Fengler 2013). However, because of often and expensive maintenance for ballast tamping and cleaning works, the ballast share can reach up to 60% in maintenance and operational hindrance costs (Esveld 2014). In addition, the rail joints (Németh and Fischer 2021, 2018) and the type of the superstructure (Jover and Fischer 2022; Jover et al. 2020, 2022; A.J.T., K., Marinkovic, D., Zehn, M. 2021; Tigh Kuchak et al. 2020; Kovalchuk et al. 2019; Czinder et al. 2021) can also influence the maintenance costs as well as the life cycle costs of the tracks.

In the twenty-first century, artificial intelligence (AI) became an effective method not only in informatics but also in the engineering disciplines (Tinoco et al. 2021; Sresakoolchai and Kaewunruen 2022). AI can be applied in the prediction and prescription analysis in transportation geotechnics. In (Tinoco et al. 2021), the authors reviewed the most relevant literature on the topic, mainly focusing on design of better earthwork projects, the prediction of jet grouting soilcrete mechanical and physical properties, and the stability level of engineering slopes.

The technical reasons for the quick residual deformations of the ballast layer lie in the properties of a grained material of crushed stones that poorly absorb the dynamic loads induced by the rolling stock. In addition, the initial inhomogeneity of ballast compaction causes inhomogeneous deformations during the tamping cycle. Thus, controlling the ballast compaction and its inhomogeneity can significantly improve the superstructure quality and the operation of the tamping machines.

The process of ballast tamping and compaction is considered in many studies. A critical review of the tamping mechanisms, challenges, and proposed solutions is presented in Guo et al. (2021). The means for improving and developing tamping methodology are offered, and advice is suggested for developing novel railway track maintenance. A numerical investigation of 3D discrete polyhedral grains under the tamping process is presented in Saussine et al. (2009). The influence of vibration frequency on the compaction level, the velocity of tamping tines during the penetration phase, and the compaction mechanism of a confined granular layer under horizontal vibrations are studied. The effects of sand intrusion into ballast after sleeper tamping on settlement characteristics of ballasted track were investigated in Kumara and Hayano (2013) using one-fifth scale model tests. The relationship of several loading cycles and settlement was found, which indicated that the initial settlement process and rate of residual settlement alter after 30% sand. The study (Zhang et al. 2014) considered the influence of large track maintenance machine operation on sleeper

supporting stiffness. It is indicated that during the maintenance operation, ballast compactness is enhanced, and the supporting stiffness increases by the tamping process. Still, the supporting stiffness decreases due to the effect of stabilizing machine. The paper (Zhou et al. 2013) presents an experimental and theoretical study of ballast compaction during the tamping process. The experimental method is based on the water-filling method. The theoretical one utilizes a discrete element analysis model of railway ballast under the loading of tamping tines. The compaction was estimated by simply counting the number of particles under the sleeper. The dynamic behavior of a railway ballast layer during tamping operation is studied in Kim et al. (2018) by using 3D DEM simulations. Three types of sleeper models in the ballast layer were considered under a series of tamping operations: lifting the sleeper, insertion of vibrating tines and packing, pulling out of tines (i.e., hammers), and settling the sleeper. The compaction was estimated by ballast porosity in different zones of the ballast bed. It was shown that the ballast was both compacted and loosened during the operations. In (Gyurkó and Nemes 2022), the authors dealt with the size effect on discrete element modeling of concrete; however, Szabó et al. (Szabó et al. 2022) investigated the 3D printing possibilities of ballast particles – that can be useful for laboratory experimental tests combined with DEM modeling of railway superstructure. A DEM and multibody dynamic simulations of ballast bed tamping are presented in Shi et al. (2020) to investigate the macro-mesoscopic motion of ballasts and the effects of tamping parameters on the mechanical qualities of ballast bed. The results show that tamping destroys the uniformity of the ballast bed, and the top layer under the sleeper and the crib are the most severely affected spaces, whose compactness increased by 7.56% and decreased by 34.77%. A similar study (Dama and Ahmadian 2020) evaluates a complete tamping cycle as defined by insertion, squeeze, hold, and withdrawal. The compactness of the ballast particles was estimated by the average number of contacts per particle. The results indicate that minor squeeze and release velocities of the tines yield better compaction, and the linear motion of the tines potentially results in better compaction than elliptical motion. The impact excitation technology was presented in the study (Liu et al. 2020a) to test and analyze the influence of the number of tamping operations performed by a tamping car on the damping and stiffness of a ballast bed. The results showed that a large machine tamping operation changed the values of the two dominant resonances and affected the longitudinal vibration transmission between the sleepers. The maximum attenuation rate between adjacent sleepers was 81.25%. The paper (Przybyłowicz et al. 2020) studies and compares the present tamping methods. The possible influence of the tamping technology on the ballast-related maintenance costs is analyzed. The material transport process is experimentally studied during the side tamping using a scale model of the ballast layer and photogrammetric measurements. A theoretical finite element model (FEM) is validated to the experimental results. The analysis of the literature on the process of ballast tamping and compaction shows that a tamping operation does not necessarily cause an increase in compaction. Thus, the ballast tamping is related to the ballast transportation in the voids under the sleeper to correct track geometry. In contrast, ballast compaction and compaction processes appear during the following track dynamic stabilization and operational loading of trains.

Ballast layer compaction in its relation to the accumulation of track settlements is discussed in Li et al. (2002). It is stated that the compaction process of the ballast layer involves not only the change of the mechanical properties but also the appearance of the residual stresses due to the interlocking of the particles into an increasingly tighter arrangement with the increasing number of repeated load cycles. The early studies on compaction-induced stresses are presented in Seed and Duncan (1986), where the increased lateral earth pressure is referred to as the “locked-in” stress. The authors in Selig and Waters (1994) show that the magnitude of residual stress in ballast can be up to 10 times higher than the stress from the external loading, depending on the loading and material properties. The mechanism of geogrid aggregate interlocking (Kwon and Tutumluer 2009) based on DEM modeling, as well as the behavior of geogrids in real (field) circumstances (Fischer 2022a, 2022b), is presented in the studies (Kwon and Tutumluer 2009; Fischer 2022a, 2022b). Dynamic cone penetrometer test results documented the field-observed stiffening and strengthening of the geogrid-reinforced base courses. A similar study (Pei and Yang 2018) presents the simulations of the compaction-induced stress development in a granular base, with and without geogrid reinforcement.

The residual stress in the geogrid increased with the number of compaction passes. The article (Geng et al. 2018) provided a method for studying the locked-in stress in rock-like material using an empirical formula for the strength of rock-like material containing locked-in stress. The equations for the influence of locked-in stress on the strength of rock-like material under uniaxial and triaxial conditions were derived based on the Mohr–Coulomb criterion and effective stress principle. The effect of locked-in stress on the mechanical properties of rocks is studied in Liu et al. 2020b using rock-like materials and nitrile rubber particles. The results show that the peak strength and elastic modulus decreased with locked-in stress and inclusion content increase. The proposed approach (Gezgin and Cinicioglu 2019) for calculating passive earth pressures considers the influence of locked-in stresses that appear during the backfill preparation. The method was based on a small-scale physical model of a retaining wall. A laboratory study (Sysyn et al. 2021) presents an investigation of locked-in stress distribution under the ballast layer along with the sleeper after the cyclic loading on the sleeper. The reasons and the mechanism of the locked-in stress distribution are analyzed. The full-scale laboratory measurement of stress distribution at different track ballast bed and substructure locations is presented in Esen et al. (2022) for evaluation of reinforced soil retaining wall system as an alternative to a conventional one. The results show that the reinforcement system reached its active state already self-standing under its self-weight and train loads that resulted in reduction of pressure in retaining walls. The active state is related to the appearance of locked-in stresses in the geogrid reinforcement. The presented studies on the processes of ballast compaction and the residual stress accumulation demonstrate that the compaction processes are usually considered in relation with volume change but not with accumulation of the stresses. Thus, the study of the influence of each factor would be a promising aim of the further studies.

The control of ballast compaction is presented in many studies. A comprehensive review of the methods of ballast layer evaluation is presented in Bold (2011). The study (Sysyn et al. 2019a) additionally shows both reviews on ballast compaction

evaluation and a method for ballast compaction evaluation using a dynamic interpretation of the measured vibration impulse response and machine learning. The technique was used for compaction evaluation after maintenance works. The best opportunities for evaluating earth structure mechanical properties are presented by geotechnical methods that exploit the information about the time of wave propagation. The application of the methods for railway ballast is submitted in Sussmann et al. (2017); Park and Miller (2008) based on surface wave measurements. The paper (Sussmann et al. 2017) describes the use of spectral analysis of surface wave for characterizing rail track ballast and foundation layers. Young's modulus variation with depth is identified within the method used to assess the tie and track support at different locations. The application of a more advanced seismic method of multi-channel analysis of surface waves is presented in Park and Miller (2008). However, both ways were applicable for evaluating fouled ballast and sub-ballast in wet and dry conditions.

Moreover, the local resolution of the surface wave methods is evidentially determined by the sleeper size that is too low for ballast compaction distribution identification along with a sleeper. The paper (Feng et al. 2021) introduces an innovative data-driven prediction approach for cross-tie support conditions from a full-scale ballasted track laboratory experiment. The discrete element method (DEM) is leveraged to provide training and testing data for the deep learning ResNet that offers high accuracy predictions. The trained model presented high accuracy from vertical acceleration measurements captured by advanced "SmartRock" sensors from a full-scale ballasted track laboratory experiment. Another approach for laboratory identification of ballast compaction distribution is presented in Sysyn et al. 2019b; Sysyn et al. 2020). The method is based on determining the wave time of flight (ToF) from the impact points on the surface to the array of the microphones and acceleration sensors under the ballast layer along with the sleeper. The results show the formation of the wave velocities gradients from the center of the sleeper to the ends. The paper (Xiao et al. 2021) presented testing results of a laboratory gyratory compaction study using real-time particle motion sensors to record particle movement characteristics during the compaction process and provide a mesoscale explanation about compaction mechanisms. It was found that the quality of compaction and the extent of particle breakage appear to be positively correlated, thus necessitating the cost-effective balance between them. The paper (Suwal et al. 2020) presents an ultrasonic measurement system for application to measure elastic waves on coarse-grained granular materials. Unlike the seismic methods, the ultrasonic ones could be a promising tool for identifying the local compaction and compaction distribution under a sleeper. The presented seismic geotechnical methods identify only the mechanical properties that are the main shortcoming of the methods regarding the consolidated ballast layer with locked-in stress. The proposed approaches for control of ballast compaction are usually used to identify the ballast elastic properties without differentiation of the stressed conditions. Therefore, there is a necessity for the development of methods for ballast stress identification.

In (Ramos et al. 2022), the authors applied a short ballasted track section with three sleepers in the laboratory at Heriot-Watt University in the UK. Their measurements and research were related to a receptance test (it was a tool to identify

the resonant frequencies that typify the dynamic behavior of the railway track, and the results can be applied in a calibration and validation procedure of a FEM/DEM model). The response of the railway track was assessed with the help of accelerometers placed on the head and web of the two rails and the sleepers. The considered railway track section was loaded with more than 3 million loading cycles, leading to the degradation of the structure. The test results provided that there was not a total overlap of the experimental curves from tests in symmetric conditions, probably because of the compaction state of the substructure and the variant settlements due to the cyclic loadings. Only the receptance tests related to the middle sleeper provided results according to the coherence limit (higher than 0.9) until the frequencies 300–400 Hz.

In (Ramos et al. 2021), the influence of track foundation on the performance of ballasted and ballastless (concrete slab) tracks under cyclic loading was taken into consideration. The authors performed experimental laboratory tests with 3 million loading cycles on a full-scale model, and they considered finite element modeling to be able to simulate the same process on a computer. The obtained results from the calibration process (short-term and long-term behavior) in the numerical modeling show good correspondence between the numerical and experimental results. During the sensitivity analysis, the Young modulus and the Poisson's ratio of the materials (railpads, ballast, frost protection layer (i.e., mainly granular supplementary layer), and subgrade) were the most relevant parameters. It was observed and stated that cohesion of the subgrade could significantly impact the permanent deformation. Therefore, predicting the permanent deformations on both types of track structures (ballasted and slab tracks) can be an adequate methodology in modeling the long-term deterioration of the track structures and transition zones.

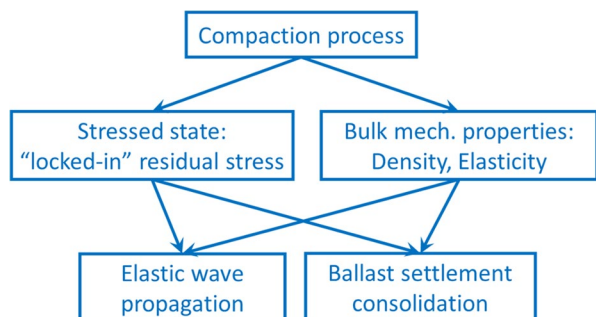
The relation of stress in granular media to elastic wave propagation is considered in the following papers. The influence of the stress history on wave velocities is studied in Cheng et al. (2020); Jia et al. 2021) using DEM simulations. The results show that p- and s-wave velocities increase under oedometric compression with confining pressure following a power law; the wave velocities vary slightly with the input frequency. The studies (Dutta et al. 2021; Dutta and Otsubo 2019) present the experimental investigation of elastic wave velocities in the specimens with different void ratios and stress. The results show that the increment of the normal stress component significantly influences compression wave velocity compared to shear wave velocity. The relation to the confinement stress is linear. The studies (Tang and Yang 2021, 2018) present the numeric investigation of factors influencing wave propagation in dry granular materials using DEM modeling. The elastic moduli and Poisson's ratio of each packing have been obtained by compression using pressure and shear wave velocities. A linear relationship has been identified between the coordination number normalized by contact force and the elastic moduli normalized by confining pressure. It was found that an increase in the aspect ratio of particles leads to a notable increase in the elastic s- and p-wave velocity, whereas for non-spherical particles with a given aspect ratio, an increased particle blockiness causes a moderate reduction in the wave velocity. The study (Li et al. 2021) uses DEM to simulate triaxial compression experiments applying spherical particles with four samples isotropically confined

at various initial packing densities and then sheared monotonically up to the critical state. The results reveal that the pressure wave is affected by the major principal stress while the shear wave velocity is more influenced by the geometric mean stress and the mean coordination number. A shear-wave velocity-based constitutive model with a critical state soil mechanics is developed in Muttashar and Bryson (2020) to predict the undrained triaxial behavior of fine-grained sediments. Laboratory tests were performed for sediment samples ranging from silt-predominant to clay-predominant sediments. A power function was proposed to describe the relationship between mean effective stress and shear-wave velocity. Most of the presented studies are based on DEM modeling that is characterized by an intensive calculation process that limits its application to relatively small samples. However, there are other promising numerical wave propagation approaches studying the whole superstructure, like described in Kurhan (2016); Kurhan and Kurhan (2019). The presented papers on wave propagation relation in granular media consider homogenous stress distribution, but the railway ballast is subjected to the locally inhomogeneous stresses and the corresponding wave propagation effects that are the problems of the further studies.

The ballast bed compaction refers to the ability to withstand the accumulation of residual deformations under the cyclic loadings after compaction. The ballast compaction process appears after the track stabilization by machines and operational loading of trains. The ballast tamping is considered in the narrow sense of tamping tines operation as the ballast transportation in the voids under the sleeper. Whereas the ballast compaction is considered equivalent to the porosity, the ballast compaction during the compaction process is accompanied on the one side by the change of the mechanical properties bulk density and on the other side by the accumulation of internal stress. Both factors influence the ballast settlement consolidation and the elastic wave propagation (Fig. 1). Therefore, the relation between the elastic wave propagation and the consolidation could provide a wave to control it and predict the residual deformations.

The present paper aims to explore the influence of the compaction process on the elastic wave propagation in the ballast layer and to study the role of internal stresses and mechanical properties. The investigation is produced using experimental laboratory measurements and numerical simulations.

Fig. 1 Influence of ballast compaction process on the ballast consolidation and the elastic wave propagation



2 Experimental Investigation of Ballast Compaction

The experimental investigation aims to simultaneously measure the stresses and wave propagation velocity in the ballast layer before and after the compaction process. Additionally, the sleeper settlement behavior is measured during the process.

The laboratory setup for the testing is presented by the 1:2.5 scaled physical model of ballast and sleeper (Fig. 2). The ballast is filled between the side walls of the box are thick-walled glass plates to form the ballast prism of the initial height of 27 cm with the slopes. The ballast material is the crushed stone of granite with a fraction 8–26 mm similar to a real particle size distribution line in scaled form. The sleeper is presented by a $1.0 \times 0.1 \times 0.1$ m H-beam that is externally loaded in the center.

The measurement devices are presented by pressure sensors, impact wave generation and acceleration sensors, and external loading and settlements ones. The pressure sensors are located under the sleeper beam and the ballast layer. The pressure sensors under the sleeper are 3 round pressure cells of the $\varnothing 110$ mm that are located under the beam ends and its central part. The pressure sensors under the ballast layer are 11 pressure cells with an active square area of 40×40 mm. The sensors are uniformly located along the sleeper axis. A more detailed description of the used measurement sensors is presented in Sysyn et al. 2019c. The QuantumX measurement system produces reading and digitalization of the pressure sensors.

The wave propagation velocity measurement system consists of the impact generation system and the vibration measurement one. The impact generation

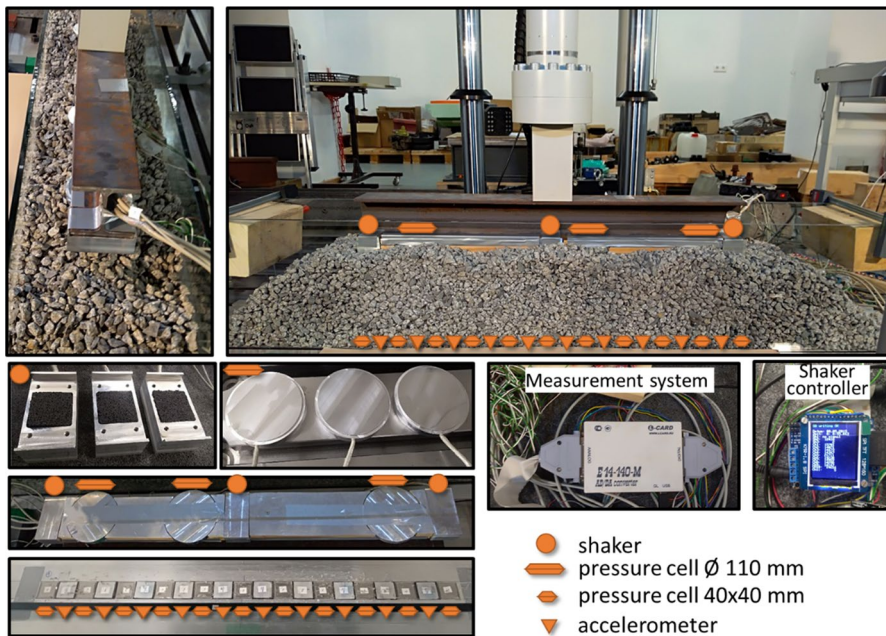


Fig. 2 Experimental setup and measurement sensors

system contains three electrodynamic shakers that are located under both ends of the sleeper and its center near the round pressure cells. The shakers are controlled by the developed microcontroller unit and power module that is programmed to produce a series of subsequent impacts on different shakers. The wave sensing is produced by 10 MEMS accelerometers ADXL335 located in isolated cases under the ballast layer along with the sleeper and the square load cells. The data acquisition of the sensor signals and the shaker contacts is produced by the measurement system E-502(LCard). More information on the wave propagation measurement is presented in Sysyn et al. 2019b; Sysyn et al. 2020).

The dynamic loading is produced by a servo-hydraulic test machine ZWICK HB 160. The loading of the machine is applied to the center of H. The vertical loading on the sleeper is controlled, and the machine sensors measure its movement. The loading cycle consists of 4-s 40-Hz vibration loading with amplitude 5 kN and 5.5 kN prescribed static preloading. The test reflects the action of the track dynamic stabilizer. The maximal ballast pressure corresponds to the regular one in situ, but the frequency 40 Hz corresponds to the worst case ballast liquefaction due to track elements' own frequency. Thus, highest compaction of the ballast and the residual stresses could be reached.

Figure 3 presents the actual measured loading and the resulting sleeper settlements. The deviation of the prescribed and the actual loading is caused by the intensive ballast settlements at the beginning of the loading and the loading fitting by servo-hydraulic machine. The diagram of the ballast settlements presents the intensive settlement accumulation. The settlement intensity decreases up to five times until the end of the loading cycle. The settlement intensities are determined as the increment of the residual settlements during one loading cycle. The

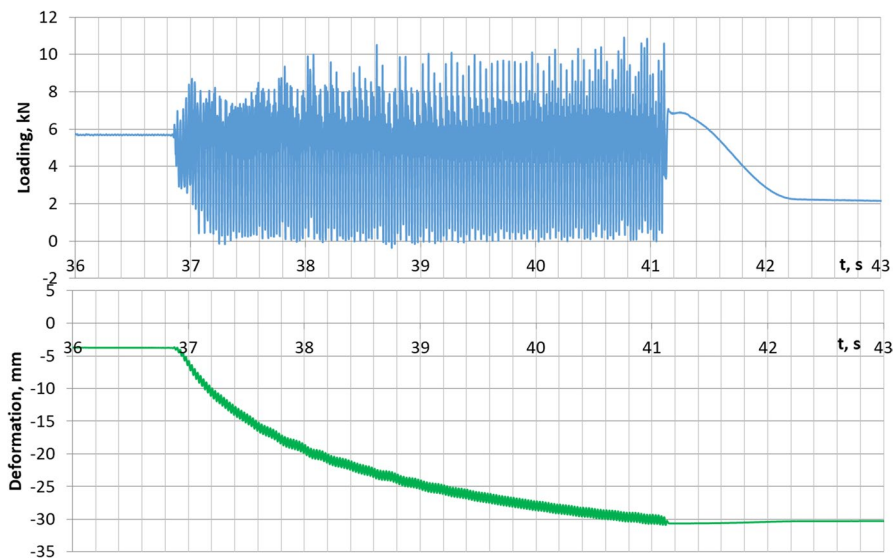


Fig. 3 Dynamic loading on the sleeper (top) and its settlements (bottom)

vertical preloading loading on the sleeper is slowly decreased after the vibration cycles.

The process of the pressure progress under the ballast layer in different sections along the sleeper is shown in Fig. 4. The average pressure on the ballast under the sleeper is proportional to the external loading and exceeds 100 kPa under dynamic cycles. The pressure decreased to zero during the unloading time. The diagrams of the pressure progress under the ballast layer in the sleeper longitudinal Sects. 0 m, 0.2 m, and 0.5 m show a similar process until the unloading part. Whereas the ballast pressure after full unloading of the sleeper in the location under the sleeper ends fully disappears, the ballast pressure under the central part of the sleeper remains. The maximal residual pressure reaches about one-third of the maximal pressure and is higher than the static preloading before the vibration cycle.

The detailed analysis of the pressure distribution maxima along the sleeper axis is presented in Fig. 5 in the three characteristic phases: preloading, vibration, and after unloading. The preloading line demonstrates more or less uniform stress distribution under the sleeper's most area, which is explained by low ballast deformations and flows. The influence of the vibration loading in the second phase is characterized by

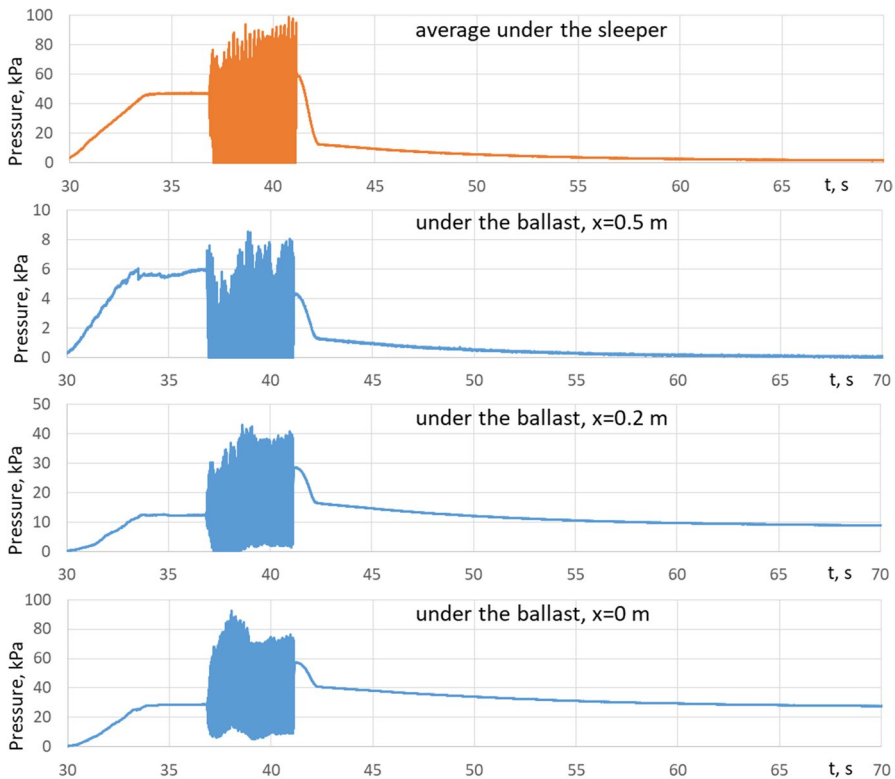


Fig. 4 The measured pressure processes under the sleeper and the ballast during the static preloading, dynamic one, and after loading

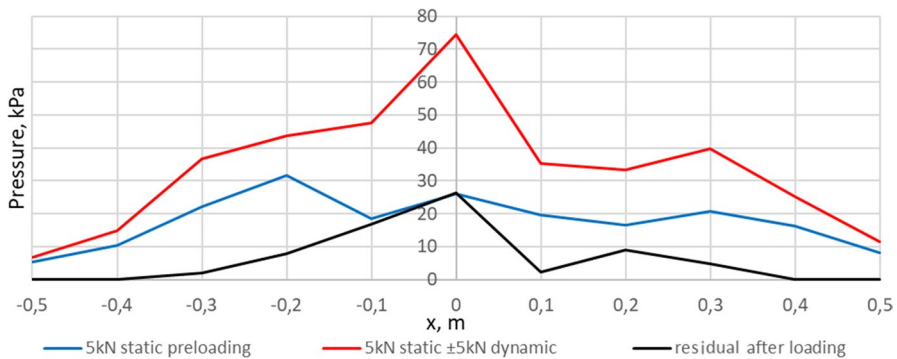


Fig. 5 The measured pressure distribution under the ballast layer along the sleeper

pressure concentration under the middle part of the sleeper. The average maximal pressure in the vibration phase is about 75 kPa compared to the average 100 kPa pressure under the sleeper, indicating the pressure distribution reduction. However, the ballast pressure under the sleeper is expected to be inhomogeneous. After the unloading phase, the residual pressure under the ballast layer appears in the zone ± 0.3 m on both sides along with the sleeper. It is characterized by the power function of pressure accumulation and depends on the horizontal pressure distribution. The measurement results correspond to the study's interlocking stress interpretation (Sysyn et al. 2021).

3 Simulation of Ballast Compaction Process and Wave Propagation Tests

The previous experimental section investigation shows that the compaction process is accompanied by the accumulation of inhomogeneous pressure distribution and the residual pressure distribution under the ballast layer. However, the experimental research does not allow studying the internal processes in the ballast layer. Therefore, the numeric simulation by discrete element modeling is used to study the influence of the ballast compaction process on wave propagation and their reasons, and the role of the locked-in stress.

The used 3D DEM model considers rolling radii, the tangential stiffness, rolling resistance coefficient, etc. The tangential force model is a Mindlin–Dersiewicz one. The normal force model is a Hertzian spring with viscous damping. The model geometrically corresponds to the experimental setup. However, the particles form is used as simple balls with an 8–26-mm standard size distribution. To be able to correct the influence of the particle form on the model parameter, the rolling resistance is calibrated together with friction and particle elasticity using the experimental results of sleeper settlements. The number of particles is 34,375. The particle material properties are the following: static friction 0.65, dynamic friction 0.6, restitution coefficient 0.72, bulk density 1600 kg/m³, Young modulus 50 GPa, Poisson ratio 0.3,

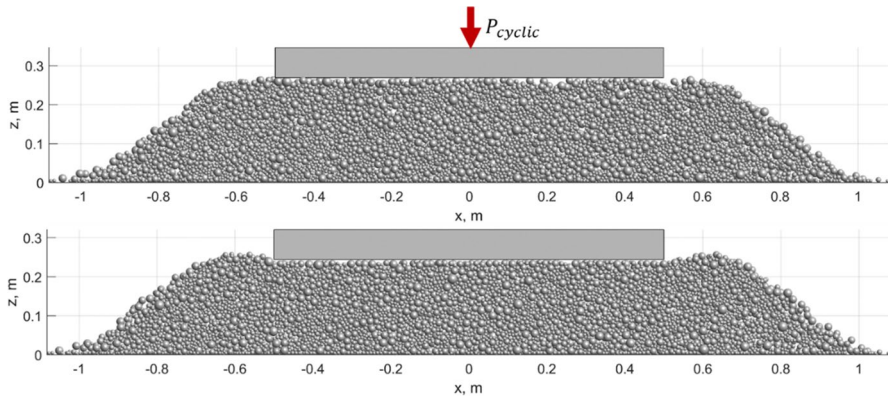


Fig. 6 DEM model of ballast bed profiles before (top) and after cyclic loading (bottom)

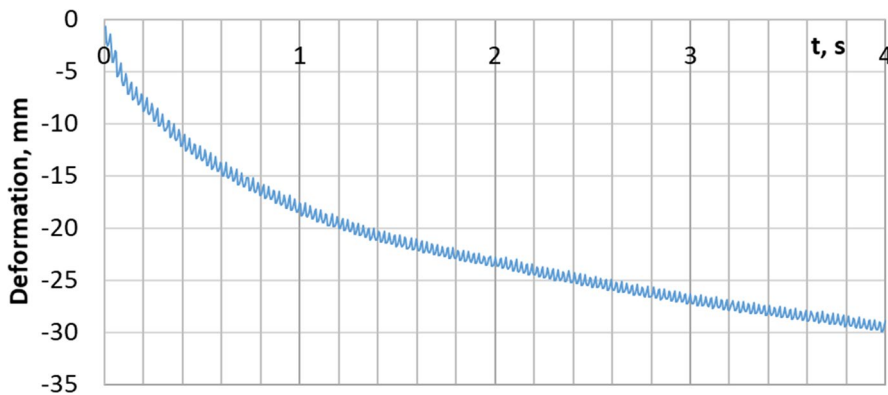


Fig. 7 Simulated settlements of the sleeper

and rolling resistance 0.32. The sleeper properties are the following: static friction 0.56, dynamic friction 0.54, restitution coefficient 0.72, density 2650 kg/m^3 , Young modulus 20 GPa, and Poisson ratio 0.3. The elastic properties of the bottom and the side walls 200 MPa were selected to correspond to the experimental conditions. The loading process on the model sleeper corresponds to the experimental one. The form of the ballast bed before and after the cyclic loading is presented in Fig. 6. The resulting sleeper settlement process (Fig. 7) is similar to the experimentally measured one and presents quick settlement accumulation intensity at the beginning of the tamping process and several times lower at the end. The overall residual settlements of the sleeper are about 30 mm, and the elastic one during the last loading cycles is about 1.2 mm. The relatively high elastic settlements are explained by the influence of the elastic subbase in the modeling and the experiment.

The distributions of the maximal normal loadings on the particles along the sleeper axis after cyclic loadings are presented in Fig. 8. The results are presented for the sleeper-ballast area Fig. 8 (top), the ballast-subgrade one Fig. 8 (center),

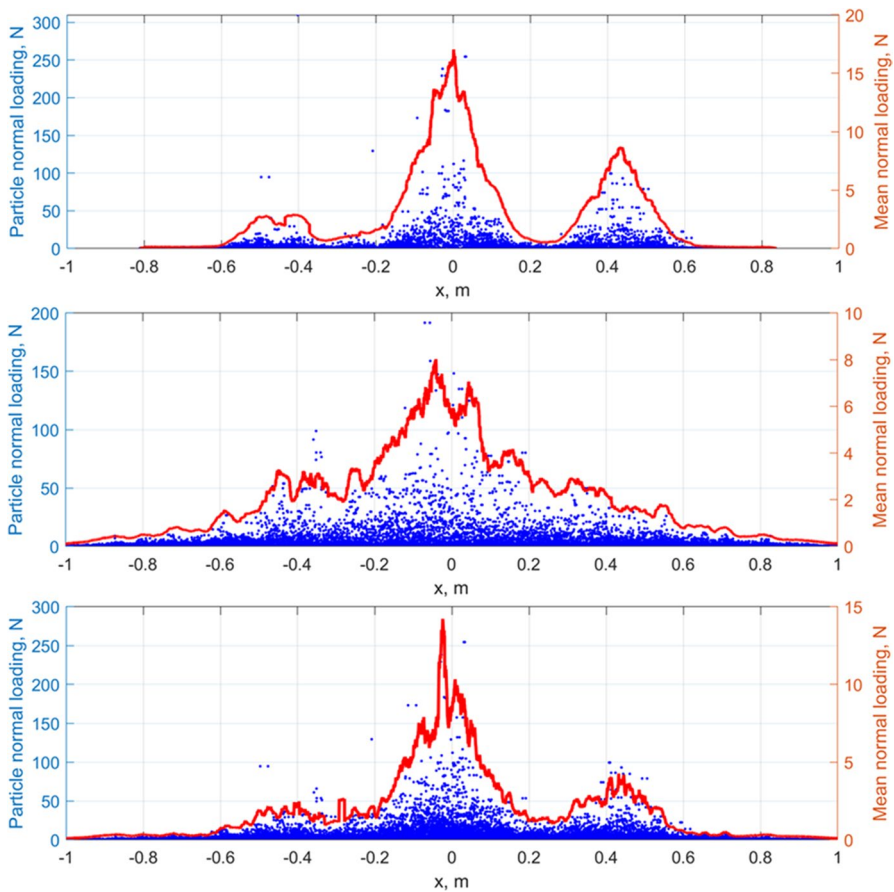


Fig. 8 Particle maximal normal loading distribution along the sleeper axis for the sleeper-ballast (top), the ballast-subgrade (centre) and whole ballast layer (bottom)

and the whole ballast layer Fig. 8 (bottom) in the fully externally unloaded sleeper. The sleeper-ballast zone (Fig. 8, top) presents the accumulation of the residual stresses in the central part of the sleeper and some accumulation zones under the sleeper ends. The residual stress accumulation under the ballast layer (Fig. 8, center) has the maximal zones in the middle part of the sleeper beam, similar to the experimental measurements (Fig. 5). Some differences to the experimental results in zones under the sleeper beam could be explained with wider shoulders of the ballast bed in the simulation model. However, the differences between the beam settlements and pressure distribution are minor and less than the regular statistical variation of the experimental measurements. The stress distribution in the whole ballast layer (Fig. 8, center) presents fewer distinct stress accumulation zones under the sleeper beam ends than for the case under the beam end, the evident zone of the stress accumulation under the central part. The

maximal observed normal loading under the central part is 2–2.5 times higher than under the sleeper ends.

The deformations of the ballast layer, excluding the subbase, are considered to estimate the average variation of the ballast mechanical properties under the sleeper beam and their following influence on the wave propagation. Figure 9 presents the elastic deformation of the ballast layer and the average elasticity during the progress of the loading cycles. The ballast box under the sleeper beam foot is approximately considered for the elastic modulus calculation. The deformation line shows that the elastic deformation amplitude decrease from 1 mm at the beginning to about 0.5 mm until 2 s, and the following deformation reduction is very slight. The elastic modulus, which depends on the ballast pressure, elastic deformation, and ballast height, variates from about 35 to 63 MPa. Thus, the relative variation of the value is about 50%. However, the form of the modulus line reflects the deformation line. It can be considered that ballast elasticity is practically constant after the initial stabilization phase.

The amount of ballast material in the volume under the beam bottom surface and along its length is studied in terms of the average ballast porosity and bulk density. Figure 10 shows that the average porosity decreases from 43.8 to 40.5%, and the ballast bulk density correspondingly increases from 1507 to 1609 kg/m³. Thus, the relative variation of the values is about 7%. Furthermore, the values change process during the vibration loading time is characterized by lower deceleration than ballast elasticity (Fig. 9).

The ballast porosity distribution along with the beam before and after compaction with the zone discretization 10 cm is shown in Fig. 11. It is clearly visible from the line after compaction the differences between the central part of the ballast and the sides where the ballast has 3% lower porosity. Despite the high variation of the values, the ballast porosity is about constant along with the beam for the case before the compaction.

The ballast compaction under the dynamic loading cause, on the one side, the double increase of the elastic modulus, and on the other – the slight increase of the material density. Assuming that the values are not depending on the internal stresses, the theoretical average pressure wave propagation velocity can be

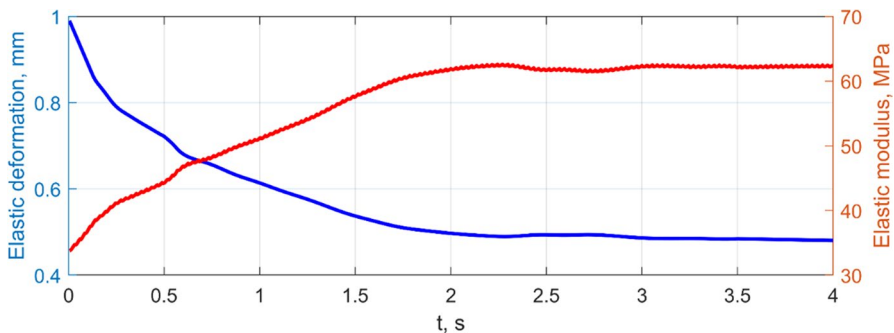


Fig. 9 Average elasticity of the ballast layer under the sleeper

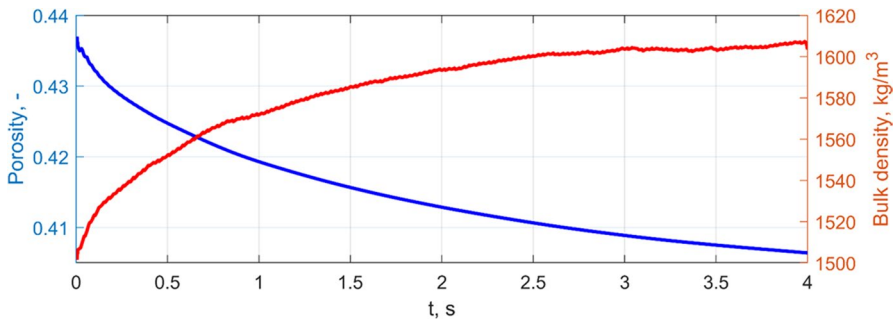


Fig. 10 Average porosity and density of the ballast layer under the sleeper

estimated using the formula $v_p = \sqrt{E/\rho}$, that is shown in Fig. 12. The pressure wave velocity increases from about 180 to 240 m/s during compaction time 2 s and afterward is constant. Thus, the increase of the wave velocity during the compaction due to the change of the mechanical properties is about 25%

As demonstrated in the experimental investigations, the ballast compaction process is characterized by appearing the residual stresses that remain after full unloading of the sleeper beam. The comparison of the normal loadings of the particles before and after the loading cycles is presented in Fig. 13. The diagram shows the homogenous distribution of the normal loading along with the beam before tamping. The local concentrations of high-loaded particles are uniformly located, and the vertical distribution reflects the weight of the particles and the sleeper beam. However, the distribution of the normal loadings after the tamping presents the concentration of the high-loaded particles under the central part of the beam. The number of the high-loaded particles quickly decreases with the distance to the beam ends. The simulation results qualitatively correspond to the measured residual stresses (Fig. 5).

The DEM model is used for modeling the wave propagation in the ballast layer. The wave is the generation by the one cycle impact loading that is applied under the center and both ends of the beam over the area 5×5 cm in a short time. The

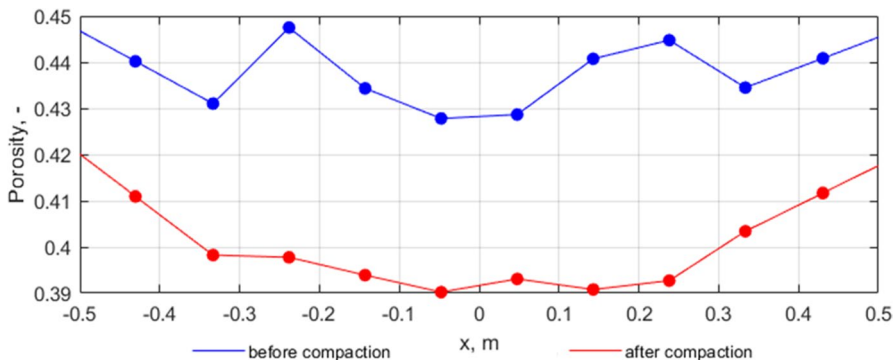


Fig. 11 Ballast porosity distribution along sleeper before and after compaction

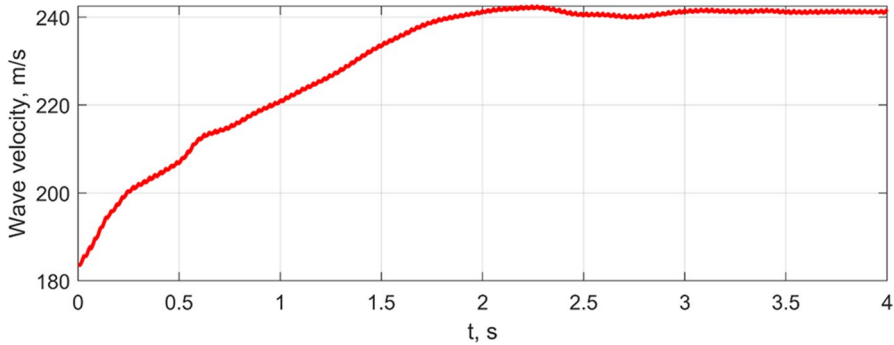


Fig. 12 Theoretical average wave propagation velocity resulting from the average bulk density and elasticity of ballast layer

propagation of wave fronts in the time moment 500 μ s before and after the cyclic loading is shown in Fig. 14. A black-red colormap shows the different absolute velocities of the particles. The particles with a velocity less than 0.5% of the maximal one are not shown.

The wave front diagram for the unconsolidated ballast (Fig. 14, top) shows a similar spherical form in all 3 locations of the sleeper beam. The front sphere radii from the impact point are about equal in all directions, demonstrating the ballast medium's homogeneity with a velocity of about 240 m/s. The wave front for the case after the cyclic loading (Fig. 14, bottom) is different from that before it in the form, size, and location. The form is characterized by corners indicating the stress transmission three that typically appears in the stressed granular material under loading. Additionally, the form is not spherical; the wavefront is stretched in the direction of the compacted zones: the side fronts are horizontally widened and the central – vertically. The wave propagation velocity under the central part of the sleeper beam is

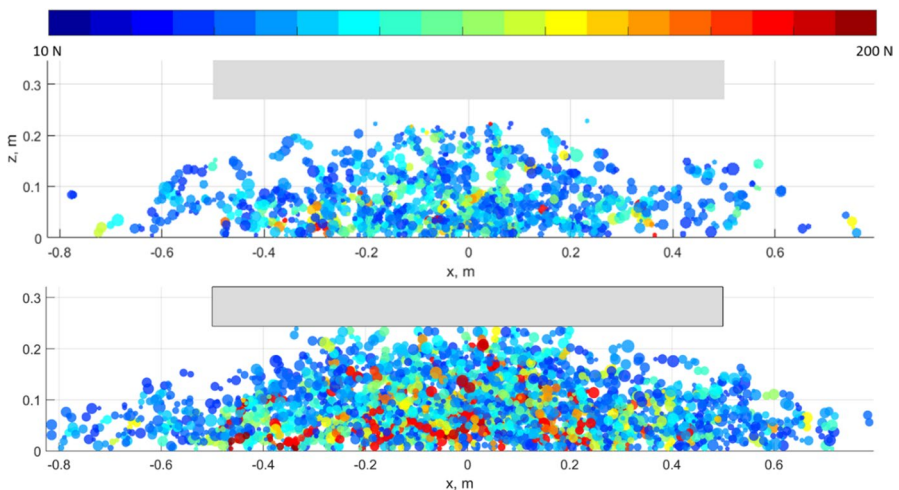


Fig. 13 Normal force in particles before (top) and after the tamping (bottom)

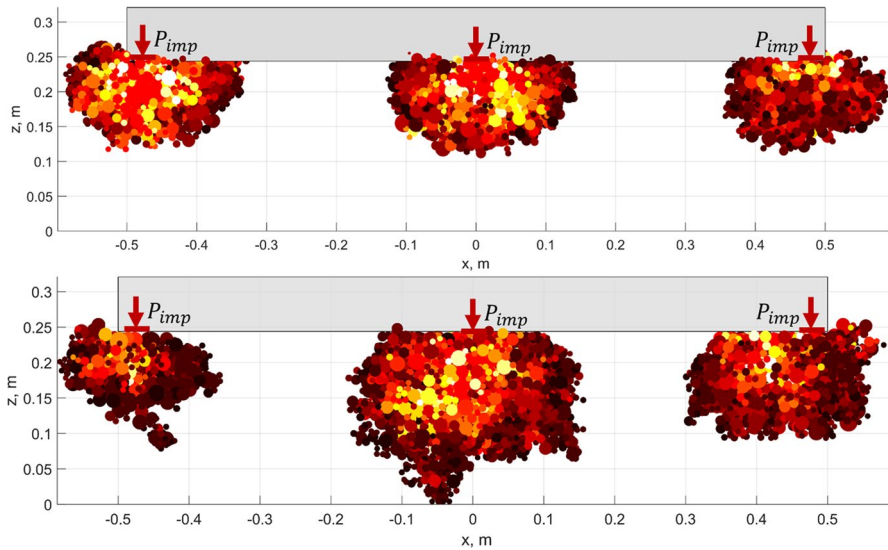


Fig. 14 Simulated wave propagation front in time moment 500 μ s after impact for unconsolidated ballast (top) and consolidated ballast after the cyclic loading (bottom)

about 520 m/s, and under the ends of the beam – 280–310 m/s. Thus, it is obvious that the wave propagation after the compaction is higher than before it.

4 Identification of Ballast Compaction Distribution Along with the Sleeper Beam

The wave propagation is measured using three shakers under the beam and the 10 acceleration sensors under the ballast layer along with the beam. The sensors that are located near the shakers can record the vibration of the shakers well enough to determine the wave time of flight. The 16 pairs of the shaker sensors or wave rays are presented in Fig. 15.

The wave propagation in the ballast under the shakers is determined from the ballast depth H and the wave time of flight from the shaker to the sensor t_{ToF} . Thereby, the determined t_{ToF} should be corrected by the constant delay time $\Delta t = 1.1$ ms that results from the properties of the low-frequency sensors ADXL355:

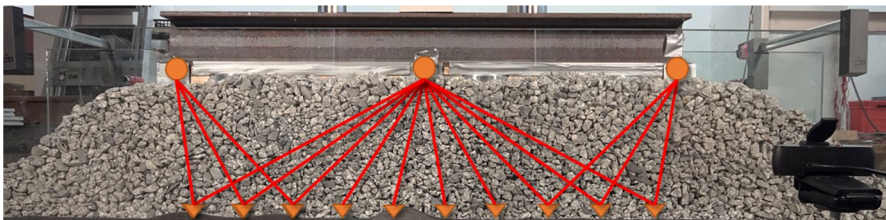


Fig. 15 Measurement scheme of the of the wave propagation velocity

$$V = \frac{H}{t_{\text{ToF}} - \Delta t} \quad (1)$$

Determining the wave velocities for the sensors that are located outside the shakers using the geometric distance between the shaker and the sensor causes the overestimation of the velocities for the inclined rays. However, the overestimation appears only after ballast compaction. The reason is the influence of the compaction gradient along with the beam that causes the refraction of wave ray if the ray is inclined (Fig. 16). Thus, the real wave path from the shaker to the sensor is longer than the geometric distance. Therefore, ray tracing is necessary during the calculation of the wave velocities for the inclined rays.

The wave refraction due to passing through the inhomogeneous medium is described by Snell's law (Margrave 2001):

$$\frac{\sin \theta_{i-1}}{V_{i-1}} = \frac{\sin \theta_i}{V_i} \quad (2)$$

The whole ray vertical path coordinates through the H zones with velocities V_i can be geometrically determined according to Fig. 16:

$$h = \Delta h_1 + \Delta h_2 + \cdots + \Delta h_i + \cdots + \Delta h_N \quad (3)$$

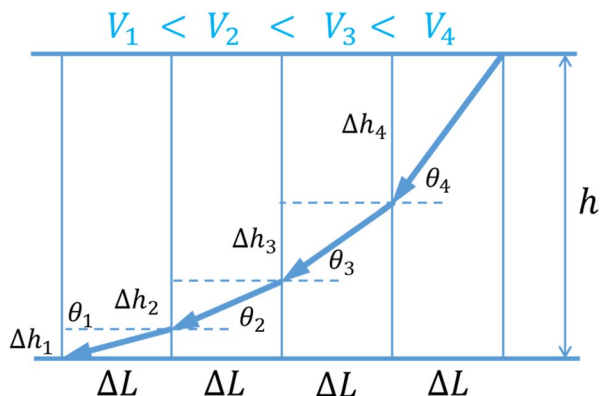
The vertical path in each zone Δh_i depends on the zone width ΔL and the ray inclination $\tan \theta_i$:

$$\Delta h_i = \Delta L \cdot \tan \theta_i = \Delta L \sqrt{\frac{\sin^2 \theta_i}{1 - \sin^2 \theta_i}} \quad (4)$$

The ray inclination $\tan \theta_i$ follows from Eq. (2):

$$\sin \theta_i = \frac{V_i}{V_{i+1}} \sin \theta_{i+1} \quad (5)$$

Fig. 16 Schematic illustration of wave propagation trace in medium with variable wave velocities



The resulting equation for the ray-tracing allows determining the first ray inclination angle θ_N based on the wave velocities V_i in each zone from the formula:

$$h = \sum_{i=1}^N \Delta L_i \sqrt{\frac{V_i^2 \cdot \sin^2 \theta_N}{V_N^2 - V_i^2 \cdot \sin^2 \theta_N}} \quad (6)$$

Figure 17 shows an example of the ray tracing in case of a stepwise distribution of the propagation waves along with the beam in 10 zones. The actual distribution of the ballast compaction along the beam is continuous; however, for identification of the velocity, the ballast bed is divided in zones of the width ΔL . Thus, the ballast compaction and the corresponding wave propagation are assumed to be constant in each zone. The identified wave paths show the significant deviation of their length from the geometrical ones for the inclined rays that pass through different zones (Fig. 18, bottom).

The wave velocity distribution for the ray tracing is unknown from the experimental measurements. It is determined by a multivariate iterative fitting of the resulting wave propagation times to the measured ones for the 16 rays together with ray tracing. Figure 18, top, presents the measured way propagation times for 16 rays. The propagation times for the side rays 1 and 16 are significantly higher than for the central one. The identified wave velocities for 10 zones along the beam (Fig. 18, bottom) demonstrate the substantial increase under the central part of the beam. The considerable variation in speed depending upon location agrees with the DEM simulation results (Fig. 14)

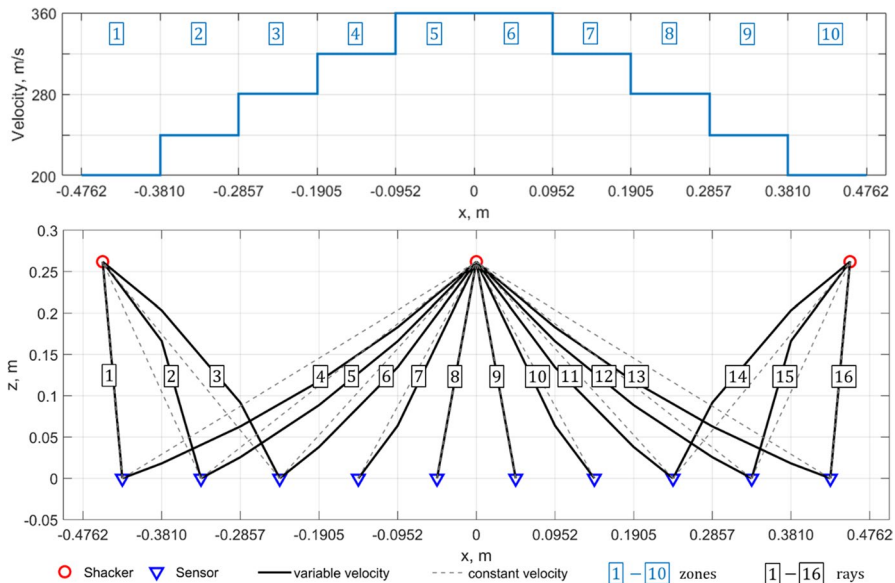


Fig. 17 Example of ray tracing for the medium with variable wave velocity zones

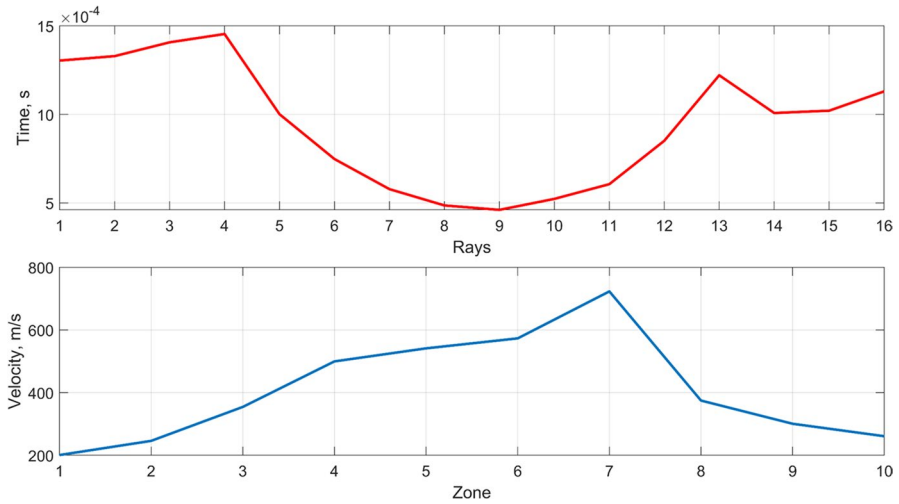


Fig. 18 The measured wave propagation times for 16 rays and the identified wave velocities in 10 zones along the sleeper

and the other previous studies (Kwon and Tutumluer 2009; Fischer 2022a). The studies (Kwon and Tutumluer 2009; Fischer 2022a) present wave propagation measurements only for three vertical rays under the middle part of the beam and both ends; however, the ToF interpretation for inclined rays produced overestimated velocity estimation using the straining path model. The present wave velocity estimation considers the wave path refraction that allows exact wave velocity estimation for the inclined rays.

The relation between the residual pressure and the pressure wave velocity is shown in Fig. 19. It demonstrates the evident increase of the wave velocity due to the ballast residual pressure in the pressure range 0–15 kPa except for two outlier points.

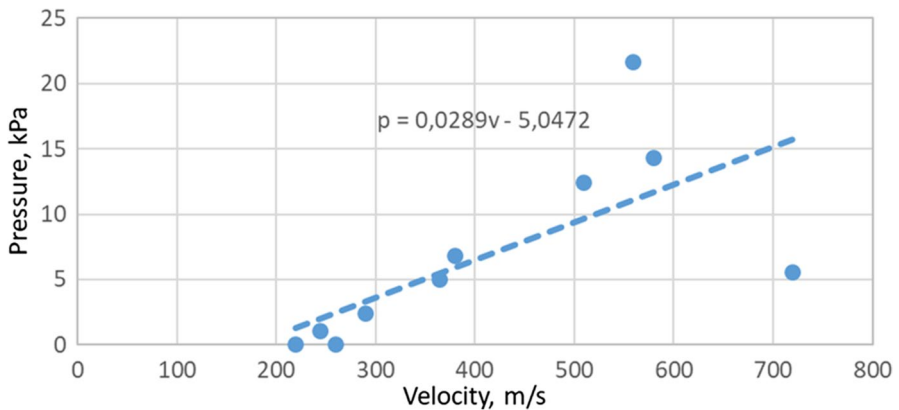


Fig. 19 Relation between the residual pressure and stress wave velocity

5 Discussion

The reviewed literature shows that the compaction process of the granular material is accompanied by both the change of the mechanical properties and the accumulation of the residual stresses. Some authors suppose appearing the stresses in the railway ballast. However, few studies exist that show the experimental measurements or theoretical simulation of the locked-in stress for railway ballast. The studies on wave propagation in granular soils indicate the significant influence of soil stresses on wave velocities. Therefore, the present study explores the possibility of ballast compaction identification using the non-destructive methods of elastic wave propagation.

The experimental measurement on the ballast compaction has shown the accumulation of the significant residual pressure under the ballast layer. The measured residual pressure is about 30% of the maximal value under the beam loading. The DEM simulation of the ballast compaction process shows a similar form of the residual pressure distribution along with the sleeper beam.

Both the measurements and simulation of the wave propagation show more than two times increase of the wave propagation velocity under the central part of the beam after ballast compaction. The increase of the velocity under the beam ends was not significant. The identified velocity distribution along the beam indicates the similarities to the residual stress distribution. However, the analysis of the simulated porosity distribution along with the beam also presents the inhomogeneous decrease of the porosity under the beam center. An estimation of the theoretical pressure wave propagation velocity is carried out to explore the influence of the material density and elasticity on the wave propagation. On the one hand, the average ballast porosity and the related density change during compaction are about 7%. On the other hand, the elastic modulus of the ballast box under the beam is increased by 50%. It is theoretically resulted in the pressure velocity increase by about 25%. The value probably should be considered the maximal one due to the possible influence of the residual pressure on the estimated elastic modulus. Moreover, both the experimentally measured and simulated wave velocity increase is 2–3 times higher. It indicates the major influence of the residual pressure on the wave propagation velocity. Similar behavior of wave propagation was presented in other experimental and theoretical studies (Sysyn et al. 2019b, 2020; Przybyłowicz et al. 2022; Kurhan and Fischer 2022).

The present study shows a qualitative estimation of the influence of possible factors on the wave propagation velocity and its relation to the residual stresses. However, future studies are necessary to clear the quantitative concerns. The influence of additional factors (like ballast and subgrade elasticity) should be studied. More deep data acquisition of the pressure and shear wave velocities would provide more information for the ballast compaction identification. Moreover, the practical application of the method on a real-life railway track is the aim of further studies. The possibilities of the wave propagation measurement with the transmitter and receiver of the ballast surface will be studied.

6 Conclusions

The following conclusions can be formulated based on the results of the present paper:

- The experimental measurement demonstrates the accumulation of residual pressure under the ballast layer and after the ballast compaction by the vibration loading on the sleeper beam.
- Both the experimental and the DEM simulations show a similar concentration form of the residual stresses under the sleeper center and quick stress release with the distance to the sleeper ends.
- The wave propagation velocity, both in the experimentally and simulations, is increased 2–3 times after the compaction.
- The wave paths for the inclined rays from transmitter to receiver along the sleeper are curvilinear due to wave refraction in the inhomogeneous medium.
- Consideration of the wave path refraction due to inhomogeneous compaction along the sleeper allows wave velocity identification for the inclined rays or in zones between the wave transmitters.
- The form of the wave velocity distribution along the sleeper is similar to the one of the residual stress distribution
- The residual pressure has a significant influence on the wave propagation velocity than the change of the mechanical properties during compaction.

Acknowledgements The authors would like to acknowledge the LCard Company for supporting the research team's work with measurement instruments.

Author Contribution M. Sysyn — conceptualization, methodology, validation, resources, project administration, and writing — original draft. U. Gerber — supervision. Jianxing Liu — investigation, visualization, software, formal analysis, and data curation. S. Fischer — writing — review and editing.

Funding Open access funding provided by Széchenyi István University (SZE).

Data Availability Data used in this research are only available upon request to the authors; in reasonable cases.

Declarations

Ethics Approval and Consent to Participate Not applicable.

Consent for Publication Not applicable.

Conflict of Interest The author declares no competing interests.

Open Access This article is licensed under a Creative Commons Attribution 4.0 International License, which permits use, sharing, adaptation, distribution and reproduction in any medium or format, as long as you give appropriate credit to the original author(s) and the source, provide a link to the Creative Commons licence, and indicate if changes were made. The images or other third party material in this article are included in the article's Creative Commons licence, unless indicated otherwise in a credit line to the

material. If material is not included in the article's Creative Commons licence and your intended use is not permitted by statutory regulation or exceeds the permitted use, you will need to obtain permission directly from the copyright holder. To view a copy of this licence, visit <http://creativecommons.org/licenses/by/4.0/>.

References

- AJT, K., Marinkovic, D., Zehn, M.: Parametric investigation of a rail damper design based on a lab-scaled model. *J Vib Eng Technol.* **9**, 51–60 (2021). <https://doi.org/10.1007/s42417-020-00209-2>
- De Bold, R.: Non-destructive evaluation of railway trackbed ballast, <https://era.ed.ac.uk/handle/1842/5027>, (2011)
- Cheng, H., Luding, S., Saitoh, K., Magnanimo, V.: Elastic wave propagation in dry granular media: effects of probing characteristics and stress history. *Int. J. Solids Struct.* **187**, (2020). <https://doi.org/10.1016/j.ijsolstr.2019.03.030>
- Czinder, B., Vásárhelyi, B., Török, Á.: Long-term abrasion of rocks assessed by micro-Deval tests and estimation of the abrasion process of rock types based on strength parameters. *Eng. Geol.* **282**, (2021). <https://doi.org/10.1016/j.enggeo.2021.105996>
- Dama, N., Ahmadian, M.: Discrete element modeling of railway ballast for studying railroad tamping operation. In: 2020 Joint Rail Conference, JRC **2020** (2020)
- Dutta, T.T., Otsubo, M.: Assessment of elastic wave velocities through granular soils during monotonic loading. In: 16th Asian Regional Conference on Soil Mechanics and Geotechnical Engineering, ARC **2019** (2020)
- Dutta, T.T., Otsubo, M., Kuwano, R.: Stress wave transmission and frequency-domain responses of gap-graded cohesionless soils. *Soils Found.* **61**, (2021). <https://doi.org/10.1016/j.sandf.2021.03.003>
- Esen, A.F., Woodward, P.K., Laghrouche, O., Connolly, D.P.: Stress distribution in reinforced railway structures. *Transp. Geotech.* **32**, (2022). <https://doi.org/10.1016/j.trgeo.2021.100699>
- Esveld, C.: Modern ack. MRT Production, Zaltbommel (2014)
- Fendrich, L., Fengler, W.: *Handbuch Eisenbahninfrastruktur*. Springer-Verlag, Berlin, Springer Vieweg (2013)
- Feng, B., Liu, Z., Tutumluer, E., Huang, H.: Data-driven railway crosstie support condition prediction using deep residual neural network: algorithm and application. *Transp. Res. Rec. J. Transp. Res. Board.* (2021) <https://doi.org/10.1177/03611981211049423>
- Fischer, S.: Geogrid reinforcement of ballasted railway superstructure for stabilization of the railway track geometry – a case study. *Geotext. Geomembranes*. GEGE103804 (2022)
- Fischer, S.: Investigation of the horizontal track geometry regarding geogrid reinforcement under ballast. *Acta Polytech. Hungarica.* **19**, (2022). <https://doi.org/10.12700/aph.19.3.2022.3.8>
- Geng, H., Xu, H., Gao, L., Chen, L., Wang, B., Zhao, X.: Elastic modulus and strength of rock-like material with locked-in stress. *Math. Probl. Eng.* **2018**, (2018). <https://doi.org/10.1155/2018/5320906>
- Gezgin, A.T., Cinicioglu, O.: Consideration of locked-in stresses during backfill preparation. *Geomech. Eng.* **18**, (2019). <https://doi.org/10.12989/gae.2019.18.3.247>
- Guo, Y., Markine, V., Jing, G.: Review of ballast track tamping: mechanism, challenges and solutions. *Constr Build Mater* **300**, 123940 (2021)
- Gyurkó, Z., Nemes, R.: Aspects of size effect on discrete element modeling of concrete. *Pollack Period.* **17**, (2022). <https://doi.org/10.1556/606.2021.00417>
- Jia, F., Cheng, H., Liu, S., Magnanimo, V.: Elastic wave velocity and attenuation in granular material. *EPJ Web Conf.* **249**, (2021). <https://doi.org/10.1051/epjconf/202124911001>
- Jover, V., Gaspar, L., Fischer, S.: Investigation of tramway line no. 1, in Budapest, Based on Dynamic Measurements. *Acta Polytech. Hungarica.* **19**, 65–76 (2022)
- Jover, V., Fischer, S.: Statistical analysis of track geometry parameters on tramway line no. 1 in Budapest. *Balt. J. Road Bridg. Eng.* **4880** (2022)
- Jover, V., Gaspar, L., Fischer, S.: Investigation of geometrical deterioration of tramway tracks. *Sci. Transp. Progress. Bull. Dnipropetr. Natl. Univ. Railw. Transp.* **0**, (2020). <https://doi.org/10.15802/stp2020/204152>

- Kim, D.S., Hwang, S.H., Kono, A., Matsushima, T.: Evaluation of ballast compactness during the tamping process by using an image-based 3D discrete element method. *Proc. Inst. Mech. Eng. Part F J. Rail Rapid Transit.* **232**, (2018). <https://doi.org/10.1177/0954409718754927>
- Kovalchuk, V., Sysyn, M., Gerber, U., Nabochenko, O., Zarour, J., Dehne, S.: Experimental investigation of the influence of train velocity and travel direction on the dynamic behavior of stiff common crossings. *Facta Univ. Ser. Mech. Eng.* **17**, (2019). <https://doi.org/10.22190/FUME190514042K>
- Kumara, J., Hayano, K.: Model tests on settlement behaviour of ballasts subjected to sand intrusion and tie tamping application. In: 18th Int Conference Soil Mech Geotech Eng: Challenges Innovations Geotechnics, ICSMGE **2013**, 1305–1308 (2013)
- Kurhan, D.M.: The basis of mathematical description for wave model of stresses propagation in railway track. *Sci. Transp. Progress. Bull. Dnipropetr. Natl. Univ. Railw. Transp.* **0**, (2016). <https://doi.org/10.15802/stp2016/84032>
- Kurhan, D., Fischer, S.: Modeling of the dynamic rail deflection using elastic wave propagation. *J. Appl. Comput. Mech.* **8**, 379–387 (2022). <https://doi.org/10.22055/JACM.2021.38826.3290>
- Kurhan, D., Kurhan, M.: Modeling the dynamic response of railway track. In: IOP Conference Series: Materials Science and Engineering (2019)
- Kwon, J., Tutumluer, E.: Geogrid base reinforcement with aggregate interlock and modeling of associated stiffness enhancement in mechanistic pavement analysis. *Transp. Res. Rec.* (2009) <https://doi.org/10.3141/2116-12>
- Li, D., Hyslip, J., Sussmann, T., Chrismer, S.: Railway geotechnics. (2002)
- Li, Y., Otsubo, M., Kuwano, R.: DEM analysis on the stress wave response of spherical particle assemblies under triaxial compression. *Comput. Geotech.* **133**, (2021). <https://doi.org/10.1016/j.compgeo.2021.104043>
- Lichtberger, B.: Track Compendium. Eurailpress Tetzlaff-Hestra GmbH Co., Publ, Hamburg (2005)
- Liu, J., Wang, P., Liu, G., Xiao, J., Liu, H., Gao, T.: Influence of a tamping operation on the vibrational characteristics and resistance-evolution law of a ballast bed. *Constr. Build. Mater.* **239**, (2020). <https://doi.org/10.1016/j.conbuildmat.2019.117879>
- Liu, X., Geng, H., Xu, H., Yang, Y., Ma, L., Dong, L.: Experimental study on the influence of locked-in stress on the uniaxial compressive strength and elastic modulus of rocks. *Sci. Rep.* **10**, (2020). <https://doi.org/10.1038/s41598-020-74556-1>
- Margrave, G.F.: Numerical methods of exploration seismology with algorithms in MATLAB. Book. (2001)
- Muttashar, W.R., Bryson, L.S.: Constitutive model for predicting stress-strain behavior of fine-grained sediments using shear-wave velocity. *Mar. Georesources Geotechnol.* **38**, (2020). <https://doi.org/10.1080/1064119X.2019.1640815>
- Németh, A., Fischer, S.: Investigation of glued insulated rail joints with special fiber-glass reinforced synthetic fishplates using in continuously welded tracks. *Pollack Period.* **13**, 77–86 (2018). <https://doi.org/10.1556/606.2018.13.2.8>
- Németh, A., Fischer, S.: Investigation of the glued insulated rail joints applied to CWR tracks. *Facta Univ Ser Mech Eng* **19**, 681–704 (2021). <https://doi.org/10.22190/FUME210331040N>
- Park, C.B., Miller, R.D.: Roadside passive multichannel analysis of surface waves (MASW). *J. Environ. Eng. Geophys.* **13**, (2008). <https://doi.org/10.2113/JEEG13.1.1>
- Pei, T., Yang, X.: Compaction-induced stress in geosynthetic-reinforced granular base course – a discrete element model. *J. Rock Mech. Geotech. Eng.* **10**, (2018). <https://doi.org/10.1016/j.jrmge.2018.02.005>
- Przybyłowicz, M., Sysyn, M., Kovalchuk, V., Nabochenko, O., Parneta, B.: Experimental and theoretical evaluation of side tamping method for ballasted railway track maintenance. *Transp Probl* **15**, 93–106 (2020). <https://doi.org/10.21307/TP-2020-036>
- Przybyłowicz, M., Sysyn, M., Gerber, U., Kovalchuk, V., Fischer, S.: Comparison of the effects and efficiency of vertical and side tamping methods for ballasted railway tracks. *Constr. Build. Mater* **314**, 125708 (2022). <https://doi.org/10.1016/j.conbuildmat.2021.125708>
- Ramos, A., Gomes Correia, A., Calçada, R., Alves Costa, P., Esen, A., Woodward, P.K., Connolly, D.P., Laghrouche, O.: Influence of track foundation on the performance of ballast and concrete slab tracks under cyclic loading: physical modelling and numerical model calibration. *Constr. Build. Mater.* **277**, (2021). <https://doi.org/10.1016/j.conbuildmat.2021.122245>

- Ramos, A., Castanheira-Pinto, A., Esen, A., Correia, A.G., Costa, P.A., Calçada, R., Woodward, P., Laghrouche, O.: Receptance test performed on a laboratory ballasted track section. In: Lecture Notes in Civil Engineering (2022)
- Saussine, G., Azéma, E., Perales, R., Radjaï, F.: Compaction of railway ballast during tamping process: a parametric study. In: AIP Conference Proceedings (2009)
- Seed, R.B., Duncan, J.M.: FE analyses: compaction-induced stresses and deformations. *J. Geotech. Eng.* **112**, (1986). [https://doi.org/10.1061/\(ASCE\)0733-9410\(1986\)112:1\(23\)](https://doi.org/10.1061/(ASCE)0733-9410(1986)112:1(23))
- Selig, E.T., Waters, J.M.: Track geotechnology and substructure management. Thomas Telford Services Ltd., London (1994)
- Shi, S., Gao, L., Cai, X., Yin, H., Wang, X.: Effect of tamping operation on mechanical qualities of ballast bed based on DEM-MBD coupling method. *Comput. Geotech.* **124**, (2020). <https://doi.org/10.1016/j.compgeo.2020.103574>
- Sresakoolchai, J., Kaewunruen, S.: Prognostics of unsupported railway sleepers and their severity diagnostics using machine learning. *Sci. Rep.* **12**, 6064 (2022). <https://doi.org/10.1038/s41598-022-10062-w>
- Sussmann, T.R., Thompson, H.B., Stark, T.D., Wilk, S.T., Ho, C.L.: Use of seismic surface wave testing to assess track substructure condition. *Constr. Build. Mater.* **155**, (2017). <https://doi.org/10.1016/j.conbuildmat.2017.02.077>
- Suwal, L.P., Pokhrel, A., Kuwano, R.: Upgrading disk transducer to measure elastic waves on coarse-grained granular materials: development and performance revelation. *Soils Found.* **60**, (2020). <https://doi.org/10.1016/j.sandf.2020.05.010>
- Sysyn, M., Nabochenko, O., Kovalchuk, V., Przybyłowicz Michał and Fischer, S.: Investigation of interlocking effect of crushed stone ballast during dynamic loading. *Reports Mech Eng.* **2**, 65–76 (2021)
- Sysyn, M., Nabochenko, O., Kovalchuk, V., Gerber, U.: Evaluation of railway ballast layer consolidation after maintenance works. *Acta Polytech.* **59**, (2019). <https://doi.org/10.14311/AP.2019.59.0077>
- Sysyn, M., Kovalchuk, V., Gerber, U., Nabochenko, O., Parneta, B.: Laboratory evaluation of railway ballast consolidation by the non-destructive testing. *Commun. - Sci. Lett. Univ. Zilina.* **21**, (2019). <https://doi.org/10.26552/com.c.2019.2.81-88>
- Sysyn, M., Kovalchuk, V., Nabochenko, O., Kovalchuk, Y., Voznyak, O.: Experimental study of railway trackbed pressure distribution under dynamic loading. *Balt. J. Road Bridg. Eng.* **14**, (2019). <https://doi.org/10.7250/bjrbe.2019-14.455>
- Sysyn, M., Kovalchuk, V., Gerber, U., Nabochenko, O., Pentsak, A.: Experimental study of railway ballast consolidation inhomogeneity under vibration loading. *Pollack Period.* **15**, (2020). <https://doi.org/10.1556/606.2020.15.1.3>
- Szabó, B., Pásthly, L., Orosz, Á., Tamás, K.: The investigation of additive manufacturing and moldable materials to produce railway ballast grain analogs. *Frat Ed Integrità Strutt* **16**, 213–228 (2022). <https://doi.org/10.3221/IGF-ESIS.60.15>
- Tang, X., Yang, J.: Modelling wave propagation in dry granular materials. In: Trends in Mathematics (2018)
- Tang, X., Yang, J.: Wave propagation in granular material: what is the role of particle shape? *J. Mech. Phys. Solids.* **157**, (2021). <https://doi.org/10.1016/j.jmps.2021.104605>
- TighKuchak, A.J., Marinkovic, D., Zehn, M.: Finite element model updating - case study of a rail damper. *Struct Eng Mech.* **73**, 27–35 (2020). <https://doi.org/10.12989/sem.2020.73.1.027>
- Tinoco, J., Parente, M., Gomes Correia, A., Cortez, P., Toll, D.: Predictive and prescriptive analytics in transportation geotechnics: Three case studies, (2021)
- Xiao, Y., Wang, M., Wang, X., Ren, J., Wang, W., Chen, X.: Evaluating gyratory compaction characteristics of unbound permeable aggregate base materials from meso-scale particle movement measured by smart sensing technology. *Materials (Basel).* **14**, (2021). <https://doi.org/10.3390/ma14154287>
- Zhang, M.N., Wu, Y., Bin, Ma, X.C., Wang, P.: Influence of large track maintenance machine on sleeper supporting stiffness. In: Advanced Materials Research. pp. 1115–1119 (2014)
- Zhou, T., Hu, B., Sun, J.: Study of railway ballast compactness under tamping operation. *J. Appl. Sci.* **13**, (2013). <https://doi.org/10.3923/jas.2013.2072.2076>

Authors and Affiliations

Mykola Sysyn¹ · Ulf Gerber¹ · Jianxing Liu² · Szabolcs Fischer³ 

Mykola Sysyn
mykola.sysyn@tu-dresden.de

Ulf Gerber
ulf.gerber@tu-dresden.de

Jianxing Liu
jianxingliu@my.swjtu.edu.cn

- ¹ Institute of Railway Systems and Public Transport, Technical University of Dresden, 01069 Dresden, Hettnerstraße 2, Germany
- ² MOE Key Laboratory of High-Speed Railway Engineering, Southwest Jiaotong University, Chengdu 610031, China
- ³ Department of Transport Infrastructure and Water Resources Engineering, Széchenyi István University, 9026 Győr, Egyetem tér 1, Hungary